Desingularization of Periodic Vortex Sheet Roll-up*

ROBERT KRASNY[†]

*Courant Institute of Mathematical Sciences, New York University,
251 Mercer Street, New York, New York 10012*

The equations governing periodic vortex sheet roll-up from analytic initial data are desingularized. Linear stability analysis shows that this diminishes the vortex sheet model's short wavelength instability, yielding a numerically more tractable set of equations. Computational evidence is presented which indicates that this approximation converges, beyond the critical time of singularity formation in the vortex sheet, if the mesh is refined and the smoothing parameter is reduced in the proper order. The results suggest that the vortex sheet rolls up into a double branched spiral past the critical time. It is demonstrated that either higher machine precision or a spectral filter can be used to maintain computational accuracy as the smoothing parameter is decreased. Some conjectures on the model's long time asymptotic state are given. © 1986 Academic Press, Inc

1. INTRODUCTION

The purpose of this paper is to present a new approach for computing vortex sheet roll-up from periodic analytic initial perturbations. The periodically perturbed vortex sheet is an asymptotic model for the instability of a parallel shear flow to streamwise perturbations. In this model, the transition region between the two streams is approximated by a surface across which the tangential velocity component has a jump discontinuity. In recent years, progress has been made in understanding vortex sheet evolution but there are still important open questions. The basic theoretical result is the short time existence of an analytic vortex sheet (Sulem *et al.* [28]). Asymptotic analysis and numerical evidence suggest that with analytic initial data, a singularity forms in the vortex sheet at a finite critical time (Moore [19], Meiron *et al.* [17], Krasny [15]).

The present approach applies a method of desingularization to investigate the possible evolution of the vortex sheet past the critical time. This work should be viewed as experimental since there is currently no rigorous theory concerning the vortex sheet's evolution when it stops being analytic and previous numerical calculations have not converged past this time (e.g., Pullin [23], van de Vooren

[30], Krasny [15]). In pursuing these calculations we have been influenced by Corcos and Sherman [10] who advocate the use of deterministic models to study the coherent structures that occur in turbulent mixing layers. These structures persist at high Reynolds number (see the survey by Ho and Huerre [14]) and a common theme in fluid dynamics is that they can be approximated by vortex sheets embedded in ideal flow. The present numerical work aims at providing a convergent discretization of periodic vortex sheet roll-up, with the hope that this will contribute to a better understanding of the underlying physical shear layer instability.

A numerical method for the present problem should be capable of handling two difficulties that have beset previous computational studies.

1. Linear stability analysis of a flat, constant strength vortex sheet shows that the perturbation equations have solutions whose growth rate increases linearly with their wavenumber (Batchelor [4]). This short wavelength instability (called "Kelvin–Helmholtz instability") implies that the linearized initial value problem of vortex sheet evolution is ill-posed in the sense of Hadamard (Garabedian [11]). It helps to keep in mind Hadamard's original observation on the initial value problem for the Laplace equation: although with analytic initial data a unique analytic solution exists locally, that solution does not necessarily depend continuously on the initial data. A practical consequence for the present problem is that any consistent discretization of the vortex sheet equations will also have a short wavelength linear instability. In an actual computation, short wavelength perturbations are introduced spuriously by roundoff error and they may grow fast enough to destroy the calculation's accuracy. With a fixed machine precision, refining the mesh does not reduce the computational error since the discretization then resolves shorter wavelength modes which grow faster once they are perturbed by roundoff error. This difficulty can be partially overcome by filtering out the spurious roundoff error perturbations in wave number space or by using higher precision arithmetic [15]. An alternative remedy that has been investigated is to dampen the growth of small scales by locally averaging the computed solution in physical space (Moore [20]).

2. Another difficulty arises beyond the initial stage of the evolution, when the vortex sheet stops being analytic. At the critical time t_c, the vortex sheet strength has a cusp and the curvature has an infinite jump discontinuity, although the sheet's slope remains bounded and its tangent vector is continuous [19, 17, 15]. Some investigators (e.g., Higdon and Pozrikidis [13], van de Vooren [30]) have derived methods which are second or higher order accurate for sufficiently differentiable vortex sheets, but it is likely that such discretizations lose their consistency and do not converge when the singularity forms in the exact solution. D. Pullin has conjectured (private communication, 1983) that past the critical time, the vortex sheet is a double branched spiral with an infinite number of turns, and that as t_c is approached from above, the spiral vanishes in size. This idea is motivated by the study of self-similar spiral formation for initially flat vortex sheets which have a singular strength distribution (see Saffman and Baker [26], Pullin and Phillips

[22]). This suggests that the previous time dependent calculations for the present problem have also been hampered in trying to resolve the arbitrarily small spatial scales of a spiral using only a finite number of computational elements.

We adopt the viewpoint expressed by Anderson [1] in a study of an initially circular vortex sheet separating fluids of slightly different densities. The exact equations governing the vortex sheet's evolution are replaced by approximate (desingularized) equations for which the difficulties mentioned above are mitigated and which have numerically tractable solutions. The approximate equations are characterized by a smoothing parameter and the exact equations are recovered when that parameter is set to zero. Anderson's idea is to study the limit of solutions to these approximate equations as the smoothing parameter vanishes. This type of desingularization of vortex sheet evolution, also called the vortex blob method, was introduced by Chorin and Bernard [9]. The method has been applied and extended to a variety of fluid dynamical situations (see the review by Leonard [16]). Some previous alternative desingularizations of the present problem have incorporated a stabilizing physical mechanism into the model. Moore [18] has derived an evolution equation for a vortex layer of small thickness. Pozrikidis and Higdon [21] have numerically studied a periodically perturbed layer of constant vorticity. Pullin [23] has included surface tension terms in the evolution equation. Unlike these approaches, the specific form of desingularization that will be used here does not correspond precisely to a physical effect. Our approach is more analogous to the artificial viscosity method for capturing shocks in compressible flow (Richtmyer and Morton [24]) and the regularization techniques of Zabusky and Overman [32] for contour dynamics.

Section 2 introduces the vortex blob method as a way to desingularize the equations governing vortex sheet evolution. A linear stability analysis of the desingularized equations is performed. Section 3 presents roll-up calculations. Numerical evidence indicates that the present desingularization approach converges past the vortex sheet's critical time. The effect of roundoff error in a computation using a small value of the smoothing parameter is examined. Some conjectures on the vortex sheet's long time asymptotic state are given. The results are discussed in Section 4.

2. THE GOVERNING EQUATIONS

2.1. *Desingularization*

A vortex sheet embedded in two-dimensional ideal flow may be described by a curve $(x(\Gamma, t), y(\Gamma, t))$ where t is time and Γ is a Lagrangian parameter which measures the total circulation between a fixed material point and an arbitrary material point along the curve (Birkhoff [8]). Let δ be a nonnegative real number and consider the "δ equations"

$$\frac{\partial x}{\partial t} = \frac{-1}{2} \int_0^1 \frac{\sinh 2\pi(y - \tilde{y})}{\cosh 2\pi(y - \tilde{y}) - \cos 2\pi(x - \tilde{x}) + \delta^2} \, d\tilde{\Gamma}. \tag{1a}$$

$$\frac{\partial y}{\partial t} = \frac{1}{2} \int_0^1 \frac{\sin 2\pi(x - \tilde{x})}{\cosh 2\pi(y - \tilde{y}) - \cos 2\pi(x - \tilde{x}) + \delta^2} \, d\tilde{\Gamma}. \tag{1b}$$

where $x = x(\Gamma, t)$, $\tilde{x} = x(\tilde{\Gamma}, t)$, etc., and where it is understood that $x(\Gamma + 1, t) = 1 + x(\Gamma, t)$, and $y(\Gamma + 1, t) = y(\Gamma, t)$. When $\delta = 0$ the Cauchy principal value of the integrals is to be taken, and in this case, Eqs. (1a), (1b) determine the evolution of a periodic vortex sheet [8]. When $\delta > 0$ the integrals are proper and the equations are then a desingularized approximation to the vortex sheet evolution equations. The term "vortex sheet" will refer to an exact solution of Eqs. (1a), (1b) with $\delta = 0$, as opposed to an approximating curve which is the solution of these equations for some fixed value of $\delta > 0$.

A flat vortex sheet of constant strength, given by $x(\Gamma, t) = \Gamma$, $y(\Gamma, t) = 0$, is an equilibrium solution of the δ equations (1a), (1b) for all $\delta \geqslant 0$. As initial data for (1a), (1b) we shall consider

$$x(\Gamma, 0) = \Gamma + 0.01 \sin 2\pi\Gamma, \qquad y(\Gamma, 0) = -0.01 \sin 2\pi\Gamma, \tag{2}$$

which is a small amplitude perturbation of the equilibrium solution by a linear theory growing mode of the exact equations. With initial condition (2), the vortex sheet stops being analytic at the critical time $t_c \approx 0.375$, due to the formation of a singularity at $\Gamma = 0.5$ (corresponding to the point $x = 0.5$, $y = 0$) [19, 17, 15].

2.2. Linear Stability

The choice of desingularization made here allows an explicit linear stability analysis to be performed which gives insight into the nature of the approximation. Consider the flat, constant strength vortex sheet with a small perturbation,

$$x(\Gamma, t) = \Gamma + x'(\Gamma, t), \qquad y(\Gamma, t) = y'(\Gamma, t). \tag{3}$$

Substituting expressions (3) into Eqs. (1a), (1b), expanding the denominator and retaining only the terms which are linear in x' and y', we obtain the following linear equations for the perturbation functions (dropping the primes):

$$\frac{\partial x}{\partial t} = -\pi \int_0^1 \frac{y - \tilde{y}}{1 - \cos 2\pi(\Gamma - \tilde{\Gamma}) + \delta^2} \, d\tilde{\Gamma}. \tag{4a}$$

$$\frac{\partial y}{\partial t} = -\pi \int_0^1 \frac{(x - \tilde{x})(1 - (1 + \delta^2) \cos 2\pi(\Gamma - \tilde{\Gamma}))}{(1 - \cos 2\pi(\Gamma - \tilde{\Gamma}) + \delta^2)^2} \, d\tilde{\Gamma}. \tag{4b}$$

ROBERT KRASNY

Solutions of the form $x = Xe^{2\pi(\omega t + ik\Gamma)}$ and $y = Ye^{2\pi(\omega t + ik\Gamma)}$ exist, with constants X and Y, when the following relations hold:

$$2\omega X = -Y \int_0^1 \frac{1 - e^{2\pi ik\Gamma}}{1 - \cos 2\pi\Gamma + \delta^2} \, d\Gamma, \tag{5a}$$

$$2\omega Y = -X \int_0^1 \frac{(1 - e^{2\pi ik\Gamma})(1 - (1 + \delta^2)\cos 2\pi\Gamma)}{(1 - \cos 2\pi\Gamma + \delta^2)^2} \, d\Gamma. \tag{5b}$$

The integrals may be evaluated by the residue theorem, yielding the dispersion relation

$$\omega^2 = \frac{k(1 - e^{-k\cosh^{-1}(1 + \delta^2)}) \, e^{-k\cosh^{-1}(1 + \delta^2)}}{4\delta(2 + \delta^2)^{1/2}}. \tag{6}$$

The positive branch of ω (corresponding to growing perturbations) is plotted in Fig. 1 as a function of wavenumber $k \geqslant 0$ for several values of δ. For a fixed value of $\delta > 0$ there is a wavenumber k_m for which the growth rate $\omega(k_m)$ is maximum and in the limit $k \to \infty$ we have $\omega(k) \to 0$. The desingularized equations therefore do not exhibit the severe short wavelength instability of the exact equations. The approximation's consistency is verified by noting that in the limit $\delta \to 0$ with a fixed value of k, we recover $\omega^2 \approx k^2/4$, the dispersion relation of the exact equations (i.e., Kelvin–Helmholtz instability).

It is interesting to compare the short wavelength behaviour of the linearized δ equations with the effect produced by various physical mechanisms. For a constant vorticity layer of finite thickness there is a certain perturbation wavenumber above which the linear growth rate is zero. Surface tension also has this effect on the linear stability of a vortex sheet. In contrast, for the related problem of
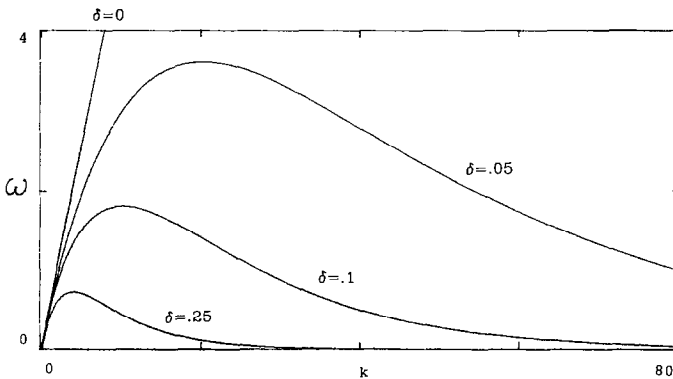

FIG. 1.   The linear dispersion relation (6) of the desingularized equations (1a), (1b) for several values of the smooting parameter ($\delta = 0.25$, 0.1, 0.05). The straight line is the dispersion relation of Kelvin–Helmholtz instability ($\delta = 0$).

Rayleigh–Taylor instability, Bellman and Pennington [6] have shown that viscosity causes the linear growth rate to vanish asymptotically with wavelength, just as occurs for the δ equations. While there may be some similarity between the effect of viscosity and the particular desingularization used here, the motivation for our approach originally came from numerical considerations for solving the $\delta = 0$ equations.

2.3. Discretization

Standard discretization techniques will be applied to solve the initial value problem (1, 2). For $0 \leqslant \Gamma \leqslant 1$ the curve $(x(\Gamma, t), y(\Gamma, t))$ is approximated by a finite number of points, $(x_j(t), y_j(t)) \approx (x(\Gamma_j, t), y(\Gamma_j, t))$, corresponding to a uniform Γ-mesh, $\Gamma_j = (j-1)\,\Delta\Gamma$, $j = 1,...N$, $N \cdot \Delta\Gamma = 1$. Trapezoidal quadrature of the integrals in (1a), (1b) yields a system of ordinary differential equations for the points' trajectories,

$$\frac{dx_j}{dt} = \frac{-1}{2N} \sum_{\substack{k=1 \\ k \neq j}}^{N} \frac{\sinh 2\pi(y_j - y_k)}{\cosh 2\pi(y_j - y_k) - \cos 2\pi(x_j - x_k) + \delta^2}, \tag{7a}$$

$$\frac{dy_j}{dt} = \frac{1}{2N} \sum_{\substack{k=1 \\ k \neq j}}^{N} \frac{\sin 2\pi(x_j - x_k)}{\cosh 2\pi(y_j - y_k) - \cos 2\pi(x_j - x_k) + \delta^2}. \tag{7b}$$

If $\delta = 0$ then (7a), (7b) is the point vortex approximation of Rosenhead [25]. The initial point positions will interpolate initial condition (2),

$$x_j(0) = \Gamma_j + 0.01 \sin 2\pi\Gamma_j, \qquad y_j(0) = -0.01 \sin 2\pi\Gamma_j. \tag{8}$$

Note that for any $\delta \geqslant 0$, Eqs. (7a), (7b) form a Hamiltonian system for the conjugate variables $x_j \cdot N^{-1/2}$, $y_j \cdot N^{-1/2}$ with the Hamiltonian function given by,

$$H(t) = \frac{-1}{4\pi N^2} \sum_{j=1}^{N} \sum_{k>j}^{N} \log (\cosh 2\pi(y_j - y_k) - \cos 2\pi(x_j - y_k) + \delta^2). \tag{9}$$

The numerical results to be presented in the next section were obtained using the fourth order Runge–Kutta method to integrate Eqs. (7), (8). The calculations were performed on a VAX 11/780 computer using, unless otherwise noted, single precision arithmetic (7 significant digits). We shall plot the point positions as well as an interpolating curve which is defined as follows. Let $p^N(\Gamma, t)$ be the trigonometric polynomial in Γ of degree $N/2$ which interpolates the computed perturbation quantities $p_j(t) = x_j(t) - \Gamma_j + iy_j(t)$ for $j = 1,..., N$. The coefficients of $p^N(\Gamma, t)$ are approximate Fourier coefficients for the periodic function $x(\Gamma, t) - \Gamma + iy(\Gamma, t)$ and are obtained by taking the fast Fourier transform of the quantities $p_j(t)$. The interpolating curve that will be plotted is the image of the function $\Gamma + p^N(\Gamma, t)$ over one period in Γ.

Following Anderson [1], we shall keep δ fixed while choosing the number of points N large enough and the time step Δt small enough to obtain an accurate solution of the δ equations (1a), (1b). By repeating this process for several values of

δ, it will be possible to say something about the limit $\delta \to 0$. We emphasize again the experimental nature of these investigations; there is presently no rigorous theory concerning this limiting process and the vortex sheet's long time existence and regularity are open problems.

3. NUMERICAL RESULTS

3.1. *Solution for* $\delta = 0.5$ *and* $\delta = 0.25$

Figure 2 shows a time sequence of the numerical solution with the value $\delta = 0.5$ for the smoothing parameter, using $N = 400$ points and a time step $\Delta t = 0.1$. The
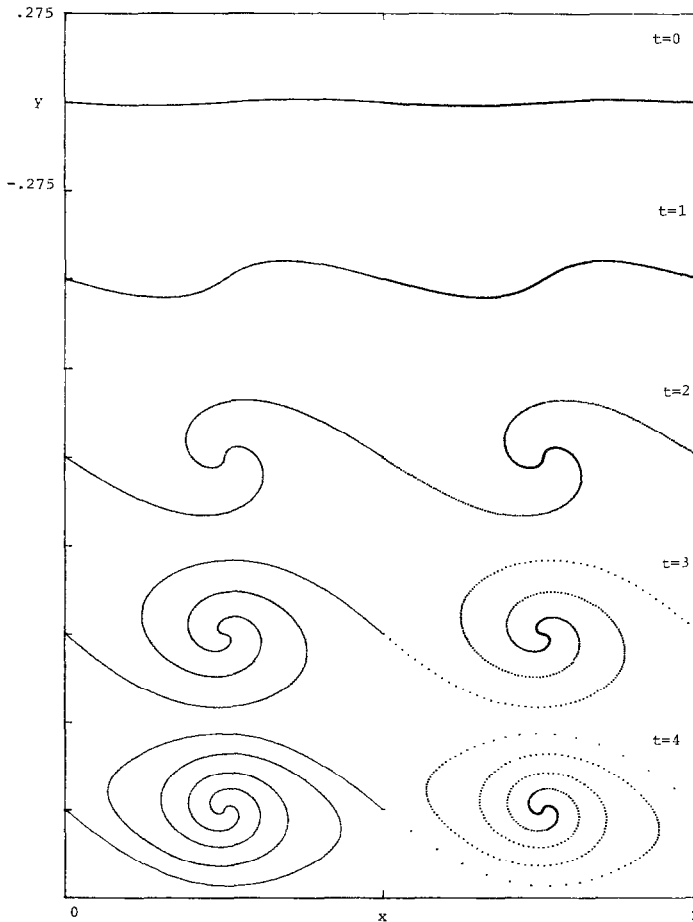
FIG. 2.   Solution of the ordinary differential equations (7), (8) with $\delta = 0.5$ and $N = 400$ at times $t = 0, 1, 2, 3, 4$. The point positions are plotted on the right side and the interpolating curves are plotted on the left.

point positions are plotted on the right side of Fig. 2 and the interpolating curve is plotted on the left. The values of N and Δt used were determined empirically and it was checked that using smaller Δt and larger N would not change the plotted curve.

The curve in Fig. 2 achieves a vertical slope between $t = 1$ and $t = 2$ and rolls up smoothly at later times. For $t > 2$ there is an inner region or core consisting of turns which become more closely spaced as time progresses. The outer region of the curve becomes elliptical in shape at late times, with the ellipse's major axis tilted slightly from the horizontal. At $t = 4$ there are two small regions of high curvature on the outer turn which are moving in opposite directions, under the influence of the free
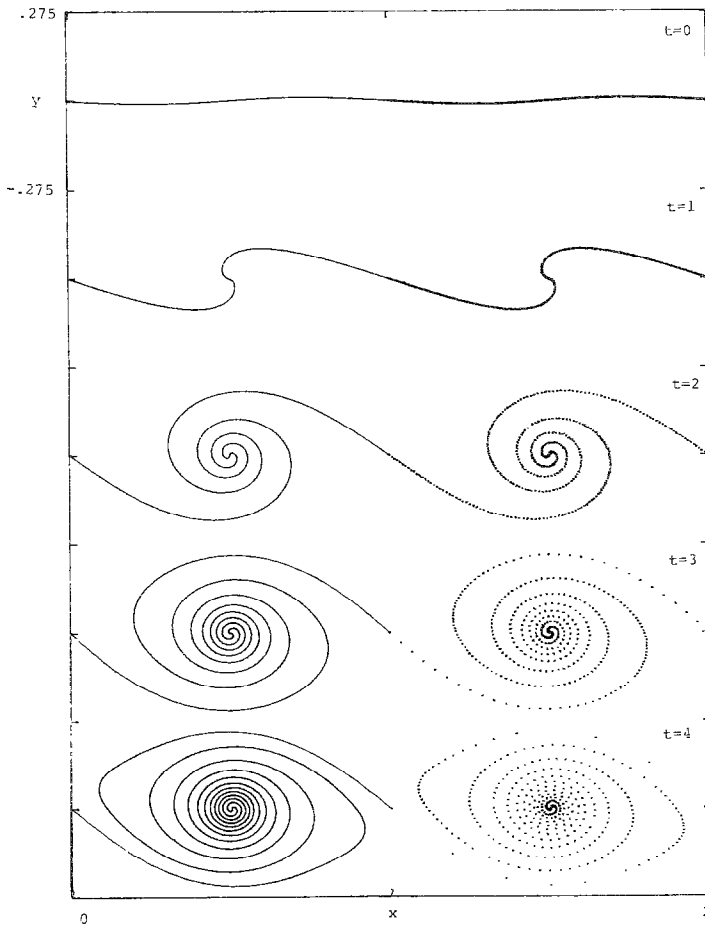

FIG. 3. Solution of the ordinary differential equations (7), (8) with $\delta = 0.25$ and $N = 400$ at successive times $t = 0, 1, 2, 3, 4$. The point positions are plotted on the right side and the interpolating curves are plotted on the left.

stream flow, toward the adjacent periods. The uneven spacing of the points on the right side of Fig. 2 indicates that the strain rate along the curve is nonuniform. The "braid" region (centered at integer values of x and connecting the cores) is most strongly stretched. As time progresses, the points travel inward along the curve's arms, being compressed near the ellipse's major axis and stretched near the minor axis.

For comparison, the calculation was repeated with $\delta = 0.25$, $N = 400$, and $\Delta t = 0.05$. The results are shown in Fig. 3. As before, the plotted curve is independent of the Γ and t meshes. In this case a vertical slope is achieved before $t = 1$. For $t \geqslant 2$ the core appears more circular than the outer region. The curvature on the outer turn at $t = 4$ reaches a value higher than that in Fig. 2 but, roughly speaking, changing the value of δ from 0.5 to 0.25 has only a small effect on the curve's outer region. With the smaller value of δ, more turns appear at the same time in the core than with $\delta = 0.5$.

Both of these calculations preserved the value of the Hamiltonian (9) to several significant digits. For example in the $\delta = 0.25$ case, $H(0) = 0.013299$ and $H(4) = 0.013303$.

3.2. Convergence in N and δ Past the Vortex Sheet's Critical Time

For a fixed value of $\delta > 0$, it was found that the curves constructed from solutions of the ordinary differential equations (7a), (7b) converge as the number of points N
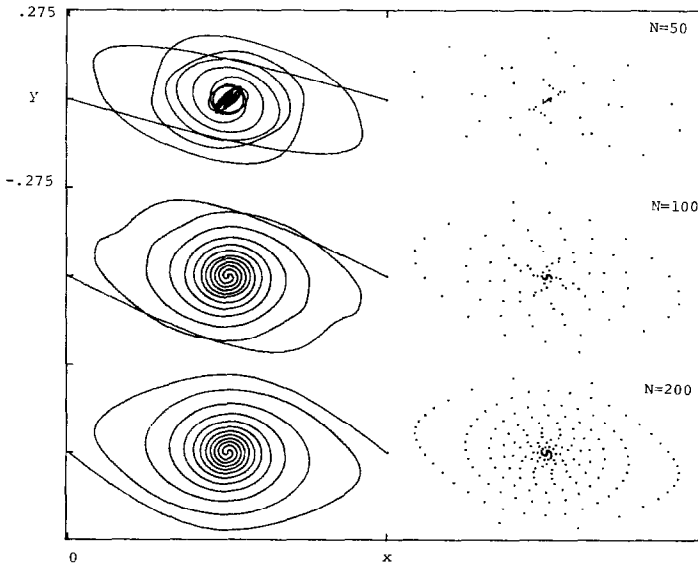

FIG. 4. Solution of the ordinary differential equation (7), (8) with $\delta = 0.25$ at $t = 4$ using $N = 50$, 100, and 200. The point positions are plotted on the right side and the interpolating curves are plotted on the left.

is increased. This convergence occurs at any time, even past the time of singularity formation in the vortex sheet ($t_c = 0.375$). Figure 4 illustrates this, showing the results at $t = 4$ for $\delta = 0.25$ with $N = 50$, 100, and 200. The time step was small enough to ensure that for each value of N the point positions are an accurate solution of Eqs. (7), (8) to within the plotting resolution. With a small value of N, the interpolating curve in Fig. 4 is tangled, but as N increases, the tangling disappears. When $N = 200$, the curve's shape has already converged to within plotting resolution as may be seen by comparison with the $N = 400$ solution in the last panel of Fig. 3. It is therefore presumed that the curves in Figs. 2 and 3 are essentially the solution of the δ equations (1), (2) for the two particular values of δ chosen, over the time interval $0 \leqslant t \leqslant 4$. Comparable accuracy can be obtained at later times by using smaller Δt and larger N.

The effect of decreasing δ at a fixed time ($t = 1$) greater than the vortex sheet's critical time ($t_c = 0.375$) is shown in Fig. 5 which plots the interpolating curve for several values of δ between 0.2 and 0.05. These calculations used $N = 400$ and
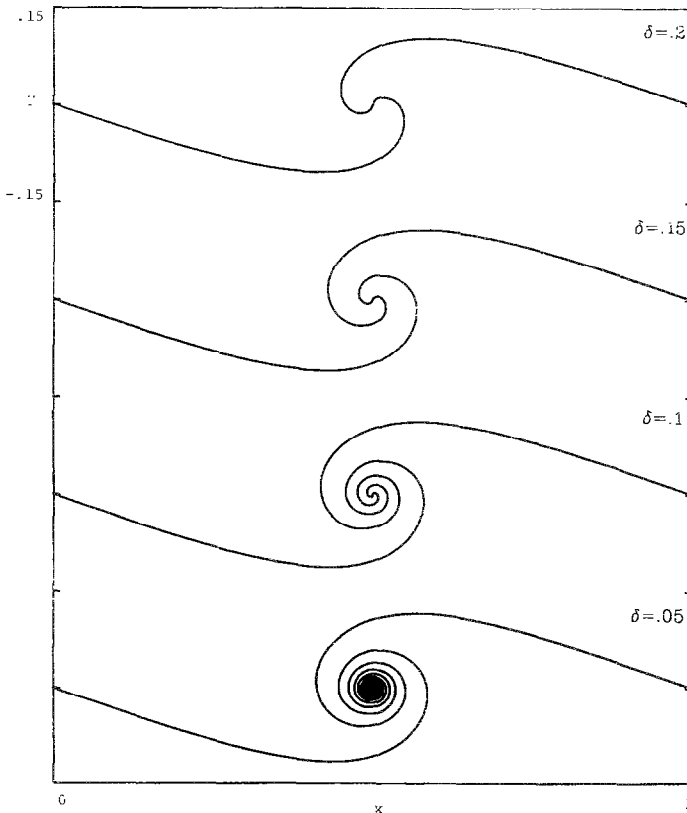

FIG. 5. Solution of the δ equations (1), (2) at $t = 1.0$ using $\delta = 0.2$, 0.15, 0.1, 0.05.
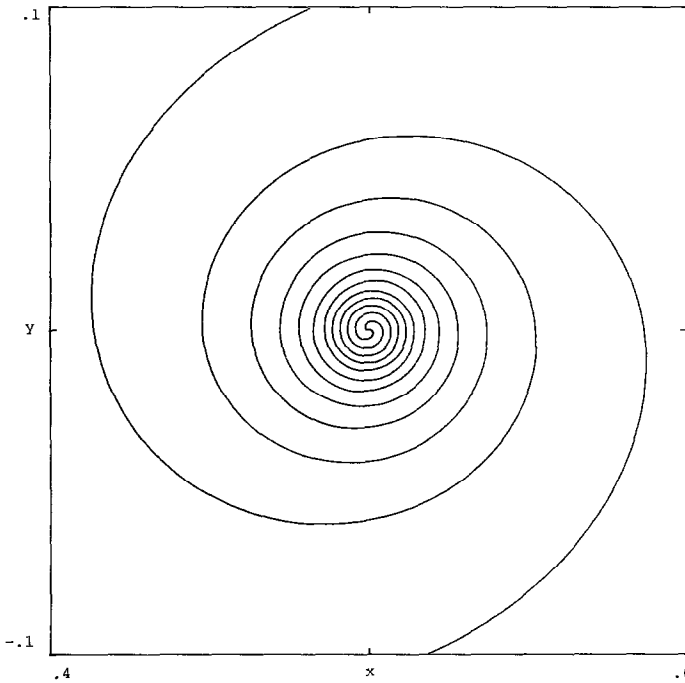
ROBERT KRASNY

FIG. 6.   An enlarged view of the inner portion of the $\delta = 0.05$ case of Fig. 5.

$\Delta t = 0.05$, except for the $\delta = 0.05$ case which used $\Delta t = 0.01$ and which was performed in double precision arithmetic (16 significant digits). The need to use greater machine precision with this smaller value of δ will be discussed later.

As δ decreases with $t = 1$ in Fig. 5, more turns appear in the core. For $\delta = 0.05$, the core region is tightly packed and an enlarged view (Fig. 6) shows that each branch of the spiral contains five complete revolutions. In Fig. 5 the curves' outer region appears to converge as δ decreases and we shall now quantify this observation. Table I contains the curves' maximum amplitude $Y_{max}(\delta)$ for various values of δ at $t = 0.5$ and at $t = 1$. These values are plotted in Fig. 7 as a function of δ, along with the polynomials in δ (quadratic in Fig. 7a, cubic in Fig. 7b) whose coefficients are determined by least squares fitting to the computed $Y_{max}(\delta)$. The good fit seen in Fig. 7 is evidence that a limiting value exists and that the error behaves like an asymptotic power series in δ as $\delta \to 0$,

$$\lim_{\delta \to 0} Y_{max}(\delta) \approx Y_{max}(0) + c_1 \delta + c_2 \delta^2 + c_3 \delta^3 + \cdots . \tag{10}$$

At $t = 0.5$ the computed $Y_{max}(\delta)$ values are well described by a quadratic function of δ for $0.05 \leqslant \delta \leqslant 0.5$. At $t = 1$, cubic dependence on δ is shown over the same interval of δ values. This suggests that the coefficients c_i in expansion (10) grow in magnitude as time increases.
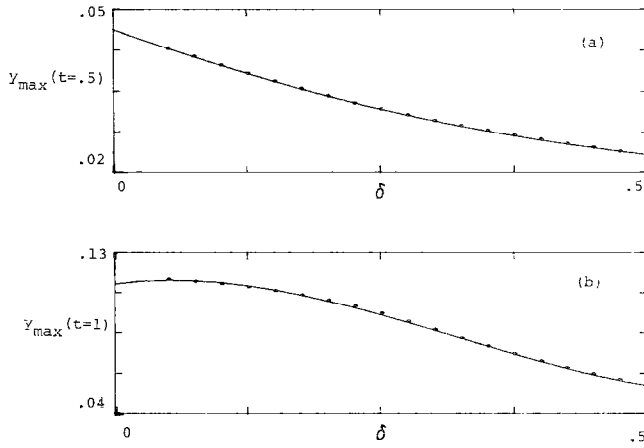
FIG. 7.   The curve's maximum amplitude Y_{max} as a function of δ. (a) $t = 0.5$. (b) $t = 1$. The plotted curve is a polynomial in δ (quadratic in (a), cubic in (b)) whose coefficients were determined by a least squares fit to the data points in Table I.
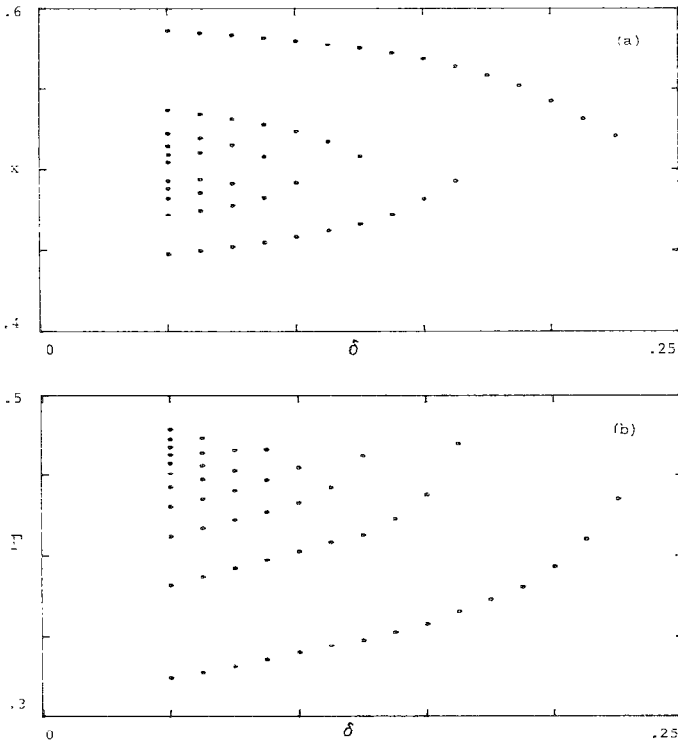

FIG. 8.   The convergence of the spiral's inner structure as δ decreases. Only one branch $(0 \leqslant \Gamma \leqslant 0.5)$ is plotted. (a) x-intercepts as a function of δ. (b) Γ values at which each intercept occurs.

TABLE I

Dependence on the Smoothing Parameter δ of
the Curve's Maximum Amplitude Y_{max}
(at $t = 0.5$ and at $t = 1$) and the Arclength L (at $t = 1$)

δ	$Y_{max} (\delta, t = 0.5)$	$Y_{max} (\delta, t = 1)$	$L (\delta, t = 1)$
0.5	0.0233	0.0561	1.034
0.475	0.0239	0.0590	1.039
0.45	0.0246	0.0622	1.044
0.425	0.0253	0.0656	1.051
0.4	0.0261	0.0693	1.059
0.375	0.0269	0.0733	1.069
0.35	0.0278	0.0776	1.082
0.325	0.0287	0.0821	1.099
0.3	0.0296	0.0868	1.123
0.275	0.0307	0.0915	1.158
0.25	0.0318	0.0960	1.207
0.225	0.0329	0.1000	1.274
0.2	0.0342	0.1034	1.358
0.175	0.0355	0.1064	1.464
0.15	0.0369	0.1088	1.601
0.125	0.0383	0.1109	1.774
0.1	0.0398	0.1128	1.996
0.075	0.0414	0.1142	2.331
0.05	0.0429	0.1155	2.790

Figure 8 contains information about how the core region behaves as δ decreases, keeping $t = 1$ fixed. In Fig. 8a we plot the curves' x-axis intercepts as a function of δ for a single branch of the spiral ($0 \leqslant \Gamma \leqslant 0.5$). For example, with $\delta = 0.1$ each spiral branch has four x-axis intercepts (see Fig. 5; the intercept at $x = 0.5$ is not included in Fig. 8). The outermost intercept approaches a value near $x = 0.6$ as $\delta \to 0$, and the next intercept on the spiral branch approaches a value near $x = 0.45$. From Fig. 8a it appears that a well defined spiral shape is emerging at $t = 1$ in the limit $\delta \to 0$. The Γ values at which the intercepts occur are plotted in Fig. 8b and they also converge. The outermost intercept ($x \approx 0.6$) approaches a Γ value near 0.3 as δ decreases. The convergence as $\delta \to 0$ is nonuniform in Γ; it occurs more rapidly further away from the spiral's center ($\Gamma = 0.5$).

The values of the curve's arclength $L(\delta)$ at $t = 1$ are also given in Table I (these values were obtained by summing the distances between consecutive pairs of points). The reciprocals $L^{-1}(\delta)$ are plotted in Fig. 9 together with the quadratic polynomial in δ determined by a least squares fit. The polynomial's value at $\delta = 0$ misses being zero by a fair margin, implying that, if the power series in δ behavior (10) is correct for $L^{-1}(\delta)$ as $\delta \to 0$, the spiral which forms in the limit $\delta \to 0$ has finite arclength.

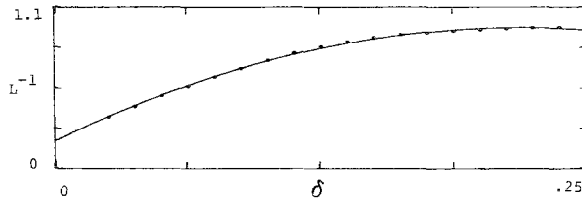Reducing δ from 0.1 to 0.05 causes a sharp increase in the number of turns in the

FIG. 9. The reciprocal of the curve's arclength at $t = 1$ as a function of δ. The plotted curve is a quadratic polynomial in δ whose coefficients were determined by a least squares fit to the values of $L^{-1}(\delta)$ obtained from Table I.

curve at $t = 1$ (Fig. 5). As the value of δ is decreased, it becomes increasingly difficult to compute accurate solutions of the δ equations since we encounter computational difficulties similar to, but not identical with, those cited in the Introduction as occuring when $\delta = 0$. At any fixed time past the vortex sheet's critical time, the curve becomes a more complicated object as δ decreases, and an accurate approximation will become more expensive, requiring larger values of N and smaller Δt. For example, the double precision $\delta = 0.05$ calculation required about 5 h to run on the VAX 11/780. This should not be taken to mean that computations using values of δ smaller than 0.05 are infeasible. The difficulty in numerically resolving such solutions could be overcome to a large extent by using a faster computer or by using more efficient adaptive Γ and t meshes instead of the uniform meshes that were used here. We consider now another difficulty affecting computations with a small value of δ that is related to, though less severe than, the loss of computational accuracy due to roundoff error that occurs in point vortex calculations for the present problem [15].

3.3 *The Effect of Roundoff Error for Small Values of δ*

Figure 10 contains time sequences of calculations with $\delta = 0.05$ that were performed in single precision (7 digit) and double precision (16 digit) arithmetic. Both calculations used $N = 400$ and $\Delta t = 0.01$. With single precision arithmetic (Fig. 10a), the interpolating curve becomes tangled for $t > 0.4$ but the tangling is absent from the double precision calculation (Fig. 10b). This tangling occurs not because of truncation error (i.e., choosing the value of N too small, as in Fig. 4 with $\delta = 0.25$ and $N = 50$ at $t = 4$) but because roundoff error introduces spurious perturbations which are amplified in time by the δ equations' dynamics.

This can be seen by examining the computed Fourier coefficients. Recall that these coefficients are obtained by taking the fast Fourier transform of the computed perturbation quantities $x_j(t) - \Gamma_j + iy_j(t)$. Figure 11 contains log-linear plots of these coefficients' amplitudes at successive times as a function of wavenumber k for both the single and double precision calculations. The initial condition (8) has nonzero Fourier coefficients only for modes $k = \pm 1$. However, as seen in the $t = 0$ plots of Fig. 11, roundoff error is present in all of the higher computational modes. At
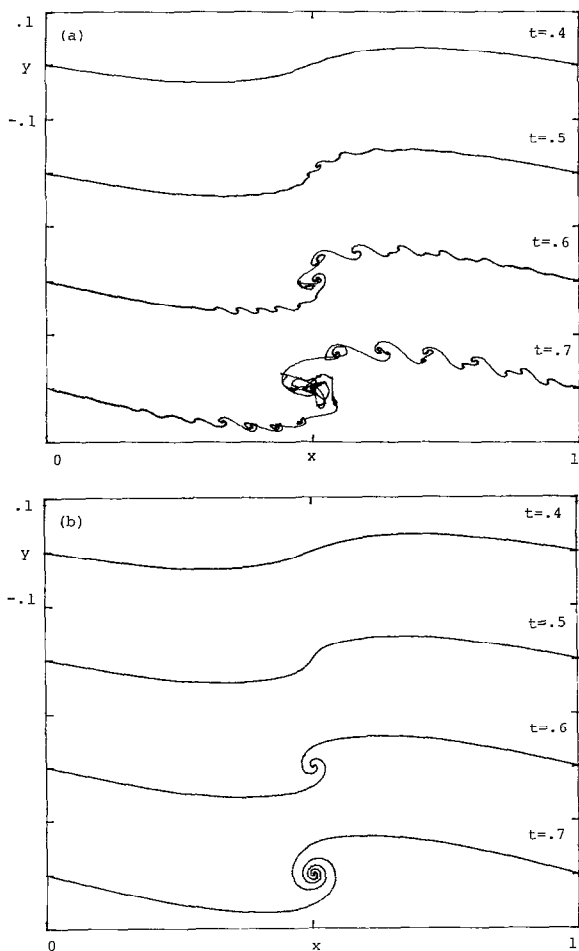
FIG. 10.   Solution of the ordinary differential equations (7), (8) with $\delta = 0.05$ and $N = 400$ at $t = 0.4$, 0.5, 0.6, 0.7. (a) Single precision arithmetic (7 digits). (b) Double precision arithmetic (16 digits). The interpolating curve is plotted in each case.

later times in single precision, the computed spectrum for $k > 10$ is jagged and its shape is roughly described by the linear dispersion relation (6) (compare Fig. 11a at $t = 0.4$ with Fig. 1). A band of intermediate wavelength modes around $k = 20$ has been amplified faster than the neighboring modes causing large inaccuracy in the computed curve of Fig. 10a for $t > 0.4$. By comparison in double precision, the computed spectrum at $t = 0.4$ remains smooth and decays in amplitude until the roundoff error level is reached (Fig. 11b). In this case the $k > 1$ modes have entered the computation legitimately, due to the effect of nonlinearity upon the initial $k = 1$ perturbation.
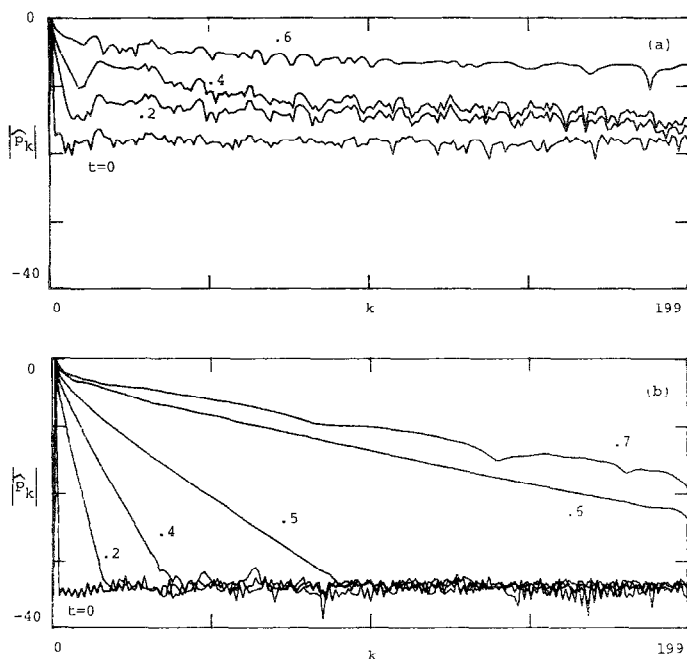
FIG. 11. Discrete Fourier coefficients of the solution in Fig. 10 ($\delta = 0.05$). The logarithm of the coefficients' amplitude is plotted against wavenumber k for several times. (a) Single precision arithmetic (7 digits). $t = 0$, 0.2, 0.4, 0.6. (b) Double precision arithmetic (16 digits). $t = 0$, 0.2, 0.4, 0.5, 0.6, 0.7.

One conclusion to be drawn from Figs. 10 and 11 is that the machine precision restricts the computational accuracy which can be achieved for a given value of the smoothing parameter δ. As $\delta \to 0$ the maximum growth rate is given by $\omega(k_m) \approx 0.2\delta^{-1}$, where $k_m \approx \delta^{-1}$ (see (6)). If the roundoff error amplitude is held constant as δ decreases, then spurious growth of the modes near k_m will occur, impairing the computation's accuracy sooner. An alternative to using higher precision arithmetic to overcome this difficulty is to filter out the roundoff error perturbations as was done for point vortex calculations [15]. After explaining how the filter works, we will demonstrate its effect on the $\delta = 0.05$ single precision calculation (Figs. 10a and 11a).

A fast Fourier transform is performed, as previously described, at the end of each time step. If the amplitude of any mode is less than 10^{-7} then that mode is reset to zero; the other modes are not disturbed. An inverse transform is then performed to adjust the point positions and the calculation proceeds to the next time step. The value 10^{-7} is the computational noise level, set so as to bound the spurious perturbations in the computed initial spectrum. Once every mode's amplitude becomes greater than the noise level, the filter is turned off and the computation proceeds normally. The resulting curve, shown in Fig. 12a, is very close to the unfiltered
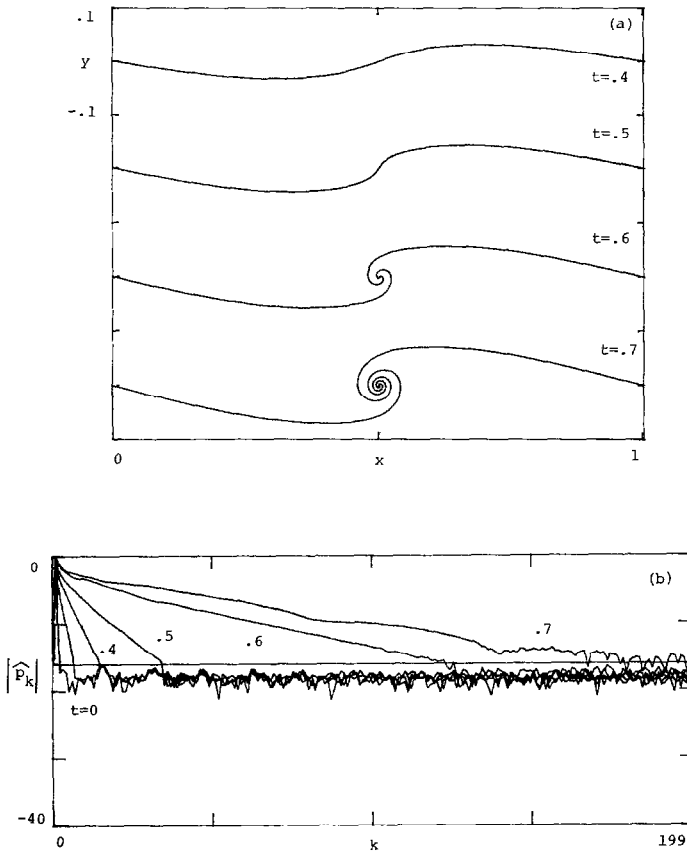
Fig. 12. A single precision calculation (7 digits) for $\delta = 0.05$ filtered at the level 10^{-7}. (a) Interpolating curve. (b) Fourier coefficients' logarithmic amplitudes. The times are the same as those in Figs. 10 and 11b.

double precision result (Fig. 10b). The computed spectrum is shown in Fig. 12b along with a horizontal line drawn at the filtering level (ln $10^{-7} \approx -16$). The filter prevents the $k > 1$ modes from entering the calculation prematurely, as had occurred in Fig. 11a. A comparison of Fig. 11b and 12b indicates that, above the computational noise level, the spectrum computed in single precision using the filter agrees well with its double precision counterpart.

3.4. Remarks on the Long Time Asymptotic State

Even though certain physical mechanisms not studied here (e.g. viscosity, pairing) become important during the long time evolution of a shear layer, it would be interesting to know the asymptotic state of the present solution. In order to get some indication about this state, we restarted the $\delta = 0.5$ calculation of Fig. 2, using $N = 4000$ points interpolated at $t = 4$ from the previously obtained $N = 400$

solution. The resulting curve and point positions are shown in Fig. 13 up to $t = 6$. The most prominent feature is that the region of high curvature on the curve's outer turn forms a "spike," crosses into the adjacent period, and continues traveling in the free stream direction. Loss of resolution in the braid region, due to the high degree of stretching taking place there, prevents us from carrying this calculation to later times. It seems plausible, however, that once a portion of the curve has left its initial period, it will never return to that period. It may also be conjectured that the inner turns successively cross the initial period's boundary at later times and that the curve becomes a highly elongated and folded ribbon. Two contrasting possibilities are that a concentrated nonzero core of circulation persists in each period, or that each period is depleted entirely of its initial circulation asymptotically as $t \to \infty$.

These remarks have bearing on an issue raised by Birkhoff and Fisher [7]. They applied the Poincaré recurrence theorem (Thompson [29]) to the Hamiltonian system (7a), (7b) in the case of point vortices, i.e., for $\delta = 0$. The theorem, however, remains relevant for $\delta > 0$. For the theorem to apply, the computational points must remain in a bounded region of phase space. Since the phase space is bounded in the horizontal direction due to periodicity, the theorem's hypothesis may be satisfied by assuming (plausibly) that the points' trajectories remain bounded in the vertical direction. The theorem's conclusion states that almost every motion of the system will return arbitrarily close to its initial configuration. Birkhoff and Fisher
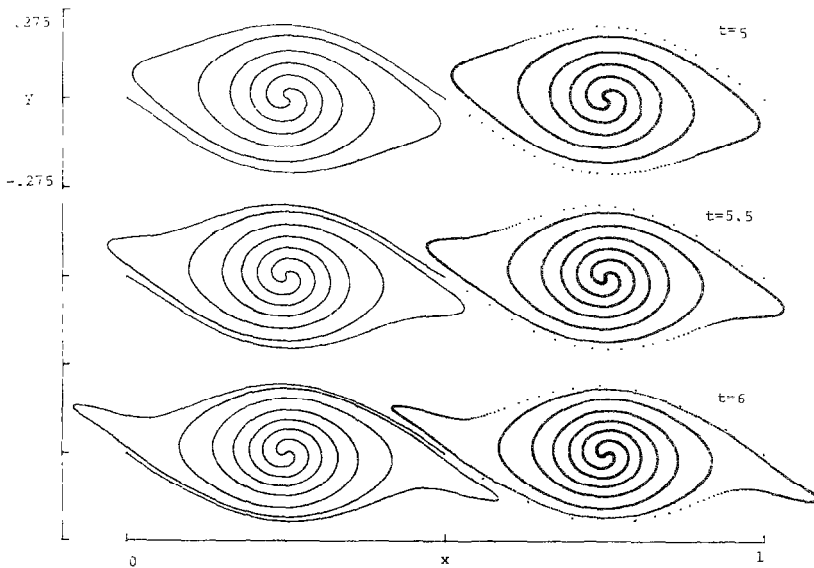

FIG. 13. Numerical solution of equations (7), (8) with $\delta = 0.5$ at times $t = 5$, 5.5, 6. This calculation was restarted at $t = 4$ with $N = 4000$ by interpolating from the $N = 400$ solution of Fig. 2. The point positions are plotted on the right side and the interpolating curves are plotted on the left.

interpreted this as implying that even if the discrete approximation rolls up after some time, it will almost surely unroll at some later time.

Figure 13, however, suggests an alternative interpretation of the theorem's conclusion, in which the points' roll-up and recurrence of their initial configuration are compatible. Any particular point may return close to its initial position in phase space either by rotating within its original period or by travelling into another period and approaching its initial coordinates shifted by an integral amount in the horizontal direction (note that physical points shifted in this manner are identical in the phase space). At a late time, the points which initially belonged to a single period may be scattered over many periods. In this way, the discrete approximation's initial configuration can recur in phase space even though the interpolating curve in physical space does not unroll.

4. DISCUSSION

As explained in the Introduction, a numerical method for vortex sheet evolution from analytic initial data must deal with two difficulties:

(1) amplification of short wavelength modes which spuriously enter the computation through roundoff error,

(2) loss of the vortex sheet's analyticity at a finite time t_c and the possible presence of a spiral in the sheet's shape at later times.

The desingularization method used here mitigates both of these difficulties. One wants to compute with a large number of points in order to better resolve the problem's small scales. For $\delta = 0$ the model's short wavelength instability restricts the number of points which can be used for a given machine precision [15]. This restriction is loosened when $\delta > 0$ since then the short wavelength modes are not violently unstable, as shown by the linear dispersion relation (6). In the computations, as long as δ was larger than 0.05, single precision arithmetic was sufficient to keep small scale irregularities due to roundoff error from forming in the curve's shape. Under these circumstances, the number of points used can be as large as the computational resources allow. When δ becomes smaller, however, care must be taken to avoid spuriously perturbing those modes whose linear growth rate is near the maximum for the particular value of δ being used. For $\delta = 0.05$ this was accomplished by using double precision arithmetic, which introduces the spurious roundoff error perturbations at a smaller amplitude. Another possible alternative that was demonstrated is to filter the spectrum at each time step. We emphasize the distinction between smoothing (i.e., putting $\delta > 0$ in Eqs. (1a), (1b)) which changes the nature of the initial value problem, and filtering (as presented here and in [15]), which ensures computational accuracy for a given machine precision as the value of δ is reduced.

Evidently for any fixed value of $\delta > 0$, the solution of the δ equations becomes,

for some $t > t_c$, a spiral with a finite number of turns. It was demonstrated in Fig. 4 that such a curve's evolution can be well approximated using a finite number of computational points. As δ approaches zero, more turns appear at a fixed time $t > t_c$ (Fig. 5). It can also be seen by comparing Figs. 2 and 3 with Fig. 10b that these turns form on a smaller scale as δ decreases. These computational results are consistent with Pullin's conjecture, already mentioned in the Introduction. Obtaining information about the spiral's inner structure which is independent of δ will require using values of δ smaller than 0.05, the smallest value used in this paper. Further work is needed to understand the relation between the singularity which forms in the vortex sheet at t_c and the spiral structure which is apparently present at later times.

Making δ positive in Eqs. (1a), (1b) mollifies the singularity that forms in the sheet's shape when $\delta = 0$. This may be surmised from Fig. 11 since the solution's approximate Fourier coefficients decay faster at $t_c = 0.375$ when $\delta > 0$ than when $\delta = 0$ [15]. For the specific purpose of studying singularity formation (i.e., for $t \leqslant t_c$), we doubt that the present approach will be more useful than the point vortex methodology discussed in [15]. Alternatively, the point vortex approximation does not converge beyond the vortex sheet's critical time and it appears necessary to use some kind of smoothing in order to study the sheet's later evolution.

The δ equations (1a), (1b) come from replacing the velocity field of a periodic row of point vortices, $(-\sinh 2\pi y, \sin 2\pi x)/2d^2$, where $d^2 = \cosh 2\pi y - \cos 2\pi x$, by that of "vortex blobs," $(-\sinh 2\pi y, \sin 2\pi x)/2(d^2 + \delta^2)$. Calculations using $((-\sinh 2\pi y, \sin 2\pi x)/2d^2)(1 - e^{-d^2/\delta^2})$, a periodic vortex blob motivated by the convergence theory of Beale and Majda [5] for smooth vorticity fields, gave qualitatively similar results. In the work of Hald [12], Beale and Majda [5], Anderson and Greengard [2], and others, the initial value problem considered is well-posed and vortex blobs are used to ensure that the discretization is consistent and stable. This contrasts with the situation for vortex sheet evolution where the effect of using vortex blobs is to replace the ill-posed initial value problem with a sequence of problems that are better behaved (though still unstable).

Bearing in mind that our computations here and in [15] necessarily use only a finite set of δ values and a finite number N of computational points, we shall make some conjectures about how the Hamiltonian system (7), (8) behaves in the two limits $N \to \infty$ and $\delta \to 0$. Calculations with point vortices ($\delta = 0$) converged as $N \to \infty$ for $t \leqslant t_c$ and they diverged as $N \to \infty$ for $t > t_c$. This divergence appeared as a tangling in the interpolating curve and it may be a sign of chaotic dynamics (see Aref [3]). By contrast, the present vortex blob calculations (keeping $\delta > 0$ fixed) converge to an untangled curve as $N \to \infty$ for any time. It seems that the two limiting processes can be interchanged without affecting the result for $t \leqslant t_c$ but not for $t > t_c$. If one first takes $N \to \infty$ and then takes $\delta \to 0$, the result is a double branched spiral for any $t > t_c$, but as already mentioned, the reverse order (first $\delta \to 0$, then $N \to \infty$) does not converge for $t > t_c$.

The smoothing parameter δ affects the allowable separation between the computational points. A consequence of the singularity that is present in the

Hamiltonian (9) when $j = k$ with $\delta = 0$ is that if the points' y coordinates remain bounded, then no pair of points can get arbitrarily close to one another (however, in the limit $N \to \infty$, the point vortices' minimum separation does approach zero [15]). For $t \leqslant t_c$ the vortex sheet is continuously differentiable, implying a bound on the small scales which are present. In this case it is apparently not necessary to allow arbitrarily close approach of the computational points for any fixed value of N since the point vortex approximation was observed to converge. Conversely, if the vortex sheet is in fact a spiral for $t > t_c$, then it contains spatial scales of all order. Putting $\delta > 0$ not only restores some control over the small spatial scales but it removes the singularity in the expression for $H(t)$, thereby allowing the computational points to approach one another even for a fixed value of N.

If one evaluates the integrals on the right-hand side of (1a) and (1b) at points not on the curve, the result (when $\delta > 0$) is a divergence free velocity field whose curl is continuous. This "vorticity" field changes in time as the curve evolves but it is not an exact solution of Helmholtz' vorticity equation. The curves computed with a fixed value of $\delta > 0$ resemble pictures of material curves in shear flow which have been obtained by other investigators. For example, our Figs. 2, 3, and 13 display features similar to the finite difference solutions of the Navier–Stokes equations obtained by Corcos and Sherman [10] and to the flow visualization obtained by Roberts, Dimotakis, and Roshko (see Van Dyke [31, p. 85]). It would be interesting to know precisely in what sense the solution of the δ equations (1a), (1b) with a fixed value of $\delta > 0$ approximates a solution of the Euler or Navier–Stokes equations.

The most important result presented here is the numerical demonstration that the desingularization approach converges past the vortex sheet's critical time, if the mesh is refined and the smoothing parameter is reduced in the proper order. While this is an improvement over previous numerical studies of periodic vortex sheet roll-up, many interesting questions remain open. Granting that solutions of the δ equations (1a), (1b) converge to a curve as $\delta \to 0$, the significance of this curve may be questioned, especially for $t > t_c$. In particular, in what sense is it a solution of the original $\delta = 0$ equation? Some authors [19, 17] have felt that the loss of analyticity at t_c implies a restriction on the validity of the vortex sheet model. This view may be unduly pessimistic when one recalls that weak solutions to other model systems (e.g., nonlinear hyperbolic equations) can be theoretically justified and remain physically relevant beyond the time of singularity formation. For the vortex sheet this raises the question of possible nonuniqueness for $t > t_c$ and the proper formulation of an "entropy" condition (see Sethian [27] for a study of these issues in relation to cusp formation for a model of flame propagation).

We hope that the computational results presented here will also stimulate further theoretical study of the vortex sheet evolution equations. In order to facilitate comparison with laboratory experiments, future computational work should try to include physical mechanisms that are neglected in the present model. An application of the ideas developed here to the vortex sheet shed by an elliptically loaded wing is in progress.

ACKNOWLEDGMENTS

REFERENCES

1. C. ANDERSON, *J. Comput. Phys.* **61**, 417 (1985).
2. C. ANDERSON AND C. GREENGARD. *SIAM J. Numer. Anal.* **22**, 413 (1985).
3. H. AREF, *Annu. Rev. Fluid Mech.* **15** (1983).
4. G. K. BATCHELOR, *An Introduction to Fluid Mechanics* (Cambridge Univ. Press. Cambridge, 1967)
5. J. T. BEALE AND A. MAJDA, *J. Comput. Phys.* **58**, 188 (1985).
6. R. BELLMAN AND R. H. PENNINGTON, *Quart. Appl. Math.* **12**, 151 (1954).
7. G. BIRKHOFF AND J. FISHER, *Rend. Circ. Mat. Palermo Ser 2* **8**, 77 (1959).
8. G. BIRKHOFF. Helmholtz and Taylor Instability, in *Proceedings of the Symposium on Applied Mathematics* (Amer. Math. Soc., Providence. RI, 1962), Vol. XIII.
9. A. J. CHORIN AND P. S. BERNARD. *J. Comput. Phys.* **13**, 423 (1973).
10. G. M. CORCOS AND F. S. SHERMAN, *J. Fluid Mech.* **139**, 29 (1984).
11. P. R. GARABEDIAN. *Partial Differential Equations* (Wiley. New York, 1964).
12. O. H. HALD, *SIAM J. Numer. Anal.* **16**, 726 (1979).
13. J. J. L. HIGDON AND C. POZRIKIDIS. *J. Fluid Mech.* **150**, 203 (1985).
14. C.-H. HO AND P. HUERRE. *Annu. Rev. Fluid Mech.* **16** (1984).
15. R. KRASNY, *J. Fluid Mech.* **167**, 65 (1986).
16. A. LEONARD, *J. Comput. Phys.* **37**, 289 (1980).
17. D. I. MEIRON. G. R. BAKER, AND S. A. ORSZAG, *J. Fluid Mech.* **114**, 283 (1982).
18. D. W. MOORE, *Stud. Appl. Math.* **58**, 119 (1978).
19. D. W. MOORE, *Proc. R. Soc. London Ser. A* **365**, 105 (1979).
20. D. W. MOORE, *SIAM J. Sci. Stat. Comput.* **2**, 65 (1981).
21. C. POZRIKIDIS AND J. J. L. HIGDON, *J. Fluid Mech.* **157**, 225 (1985).
22. D. I. PULLIN AND W. R. C. PHILLIPS, *J. Fluid Mech.* **104**, 45 (1981).
23. D. I. PULLIN, *J. Fluid Mech.* **119**, 507 (1982).
24. R. D. RICHTMEYER AND K. W. MORTON. *Difference Methods for Initial-Value Problems* (Interscience. New York, 1967), 2nd ed.
25. L. ROSENHEAD, *Proc. R. Soc. London Ser. A* **134**, 170 (1931).
26. P. G. SAFFMAN AND G. R. BAKER, *Annu. Rev. Fluid Mech.* **11** (1979).
27. J. SETHIAN, *Commun. Math. Phys.* **101**, 4 (1985).
28. C. SULEM, P. L. SULEM, C. BARDOS. AND U. FRISCH, *Commun. Math. Phys.* **80**. 485 (1981).
29. C. J. THOMPSON, *Mathematical Statistical Mechanics* (Princeton Univ. Press. Princeton, NJ, 1979).
30. A. I. VAN DE VOOREN. *Proc. R. Soc. London Ser. A* **373**, 67 (1980).
31. M. VAN DYKE, *An Album of Fluid Motion* (Parabolic Press, Stanford, CA. 1982).
32. N. J. ZABUSKY AND E. A. OVERMAN, II, *J. Comput. Phys.* **52**, 351 (1983).